**Supplementary Material**

# High-Performance Pd-Pt/$\alpha$-$MnO_2$ Catalysts for the Oxidation of Toluene

**Ning Dong [1], Wenjin Wang [2], Xuelong Zheng [2], Huan Liu [2], Jingjing Zhang [2], Qing Ye [2,*] and Hongxing Dai [3,*]**

[1] Beijing Huaneng Yangtze Environmental Technology Research Institute Co., Ltd., Beijing 102200, China; dongning2623@163.com
[2] Key Laboratory of Beijing on Regional Air Pollution Control, Department of Environmental Science, College of Environmental Science and Engineering, Beijing University of Technology, Beijing 100124, China; wwj1491721@163.com (W.W.); zxlzxl@emails.bjut.edu.cn (X.Z.); a1125700054@163.com (H.L.); zhangjj_2022@163.com (J.Z.)
[3] Beijing Key Laboratory for Green Catalysis and Separation, State Key Laboratory of Materials Low-Carbon Recycling, Laboratory of Catalysis Chemistry and Nanoscience, Department of Chemical Engineering and Technology, College of Materials Science and Engineering, Beijing University of Technology, Beijing 100124, China
* Correspondence: yeqing@bjut.edu.cn (Q.Y.); hxdai@bjut.edu.cn (H.D.); Tel.: +86-10-6739-1659 (Q.Y.); +86-10-6739-6118 (H.D.); Fax: +86-10-6739-1983 (Q.Y. & H.D.)

# Table of Contents


| Item | Page |
|---|---|
| **Catalyst characterization procedures** | 3–4 |
| **Figure S1** | 5 |
| **Figure S2** | 6 |
| **Figure S3** | 7 |
| **Figure S4** | 8 |
| **Figure S5** | 9 |
| **Figure S6** | 10 |
| **Figure S7** | 11 |
| **Figure S8** | 12 |
| **Figure S9** | 13 |
| **Table S1** | 14 |
| **Table S2** | 15 |
| **Table S3** | 16 |
| **Table S4** | 17 |

## Catalyst characterization procedures:

The actual noble metal contents of the as-obtained samples were measured using the inductively coupled plasma–atomic emission spectroscopic (ICP–AES) technique on a Thermo Electron IRIS Intrepid ER/S spectrometer. Each sample was dissolved in a mixture of concentrated HCl and $HNO_3$ aqueous solutions with a volumetric ratio of 3 : 1 prior to analysis.

The crystal phase compositions of the as-obtained samples were measured by means of the X-ray diffraction (XRD) technique on a Bruker/AXS D8 Advance diffractometer, with Cu K$\alpha$ radiation and a nickel filter ($\lambda$ = 0.15406 nm). The surface areas of the as-prepared samples were determined using the BET method via $N_2$ adsorption at –196 $^{o}$C on a Micromeritics ASAP 2020 analyzer. All of the samples were degassed at 300 $^{o}$C for 2.5 h under vacuum prior to measurement. The specific surface areas of the samples were calculated with the Brunauer–Emmett–Teller (BET) method, the pore size distributions were calculated with the DFT method based on the whole adsorption data, and the average pore sizes were calculated with the Barrett–Joyner–Halenda (BJH) method.

Scanning electron microscopy (SEM) was used to observe the morphologies of the catalyst particles. The SEM photographs of the catalysts at different magnifications were taken on a HITACHI S-4300 scanning electron microscope from Hitachi, Japan, operated at 10 kV. A JEOL-2010 transmission electron microscope (TEM) from Japan Electronics Corporation (JEOL) was used to measure the structures of the samples, and the crystalline types of the samples were determined using the selected area electron diffraction (SAED) technique. High-angle annular dark field–scanning transmission electron microscopy (HAADF–STEM) images and energy-dispersive X-ray spectroscopic (EDS) element mappings of the samples were acquired on the equipment FEI G2 80−200/Chemi−STEM Cs-corrected transmission electron TEM with probe corrector.

X-ray photoelectron spectroscopic (XPS) spectra of the samples were determined using an X-ray photoelectron spectrometer, model ESCALAB250Xi, from Thermo Fisher Scientific, USA, with a Mg K$\alpha$ ($hv$ = 1253.6 eV) excitation source, a voltage of 15 kV, a power of 250 W, a vacuum chamber pressure of $2 \times 10^{-7}$ Pa, and an acquisition step of 0.1 eV, and the

contaminant carbon peak (C 1s = 284.8 eV) was used to calibrate the shift in binding energy. The Avantage software was used to perform the curve fitting of the XPS spectra of the samples. The XPS peak deconvolution parameters are summarized in Tables S1−S4 of the Supplementary Material. It should be noted that XPS is a surface-sensitive technique that typically probes to a depth of only 5−10 nm of the material. The XRF and EDS techniques, however, have a detection depth of up to micrometers and are able to provide information on the bulk composition of the material. It has been generally accepted that the surface and bulk compositions of a material are not the same. Furthermore, the surface composition is more important than the bulk composition in catalysis. Therefore, we did not compare the surface compositions of the samples measured with the XPS technique with their bulk compositions measured by the XRF/EDS techniques. Hydrogen temperature-programmed reduction ($H_2$-TPR) tests were performed on a Chemisorption Meter Model JW-BK132 manufactured by Jingwei Gao Bo.

In the thermogravimetric (TG) experiments, a German NETZSCH STA 449 F5 simultaneous thermal analyzer (DSC/DTA-TG) was used to study the thermal stability of the samples. A total of 15 mg of the sample was used in each test, and the weight loss curves of the samples were recorded in the temperature range of 30–900 ℃ at a ramp of 10 ℃/min, and the gas passed through the sample was air with a flow rate of 50 mL/min.

The in situ diffuse reflectance infrared Fourier transform spectra (in situ DRIFTS) of the samples were recorded using a Bruker Tensor II infrared adsorption instrument. The instrument was equipped with an MCT detector and a Harrick in situ cell. Powdered samples were used and placed on a copper grid in the in situ cell. Before the test, the samples were pretreated at 400 ℃ under $N_2$ atmosphere for 1 h. Then the temperature was reduced to the required temperature and stabilized for 10 min, and the background of the samples was collected under $N_2$ atmosphere, after which the reaction gas was passed into the samples, and the spectra of the samples were collected. The spectra were collected in the range of 4000–800 $cm^{-1}$ with a resolution of 4 $cm^{-1}$ and 64 scans. The total ventilation flow rate was maintained at 50 mL/min.

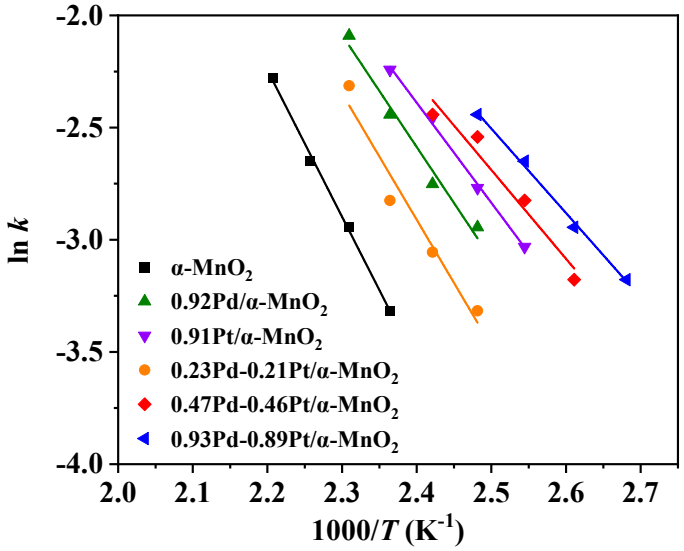



**Figure S1.** Arrhenius plots for toluene oxidation over the $\alpha$-$MnO_2$, 0.92Pd/$\alpha$-$MnO_2$, 0.91Pt/$\alpha$-$MnO_2$, and *x*Pd-*y*Pt/$\alpha$-$MnO_2$ samples at SV = 60,000 mL/(g h).

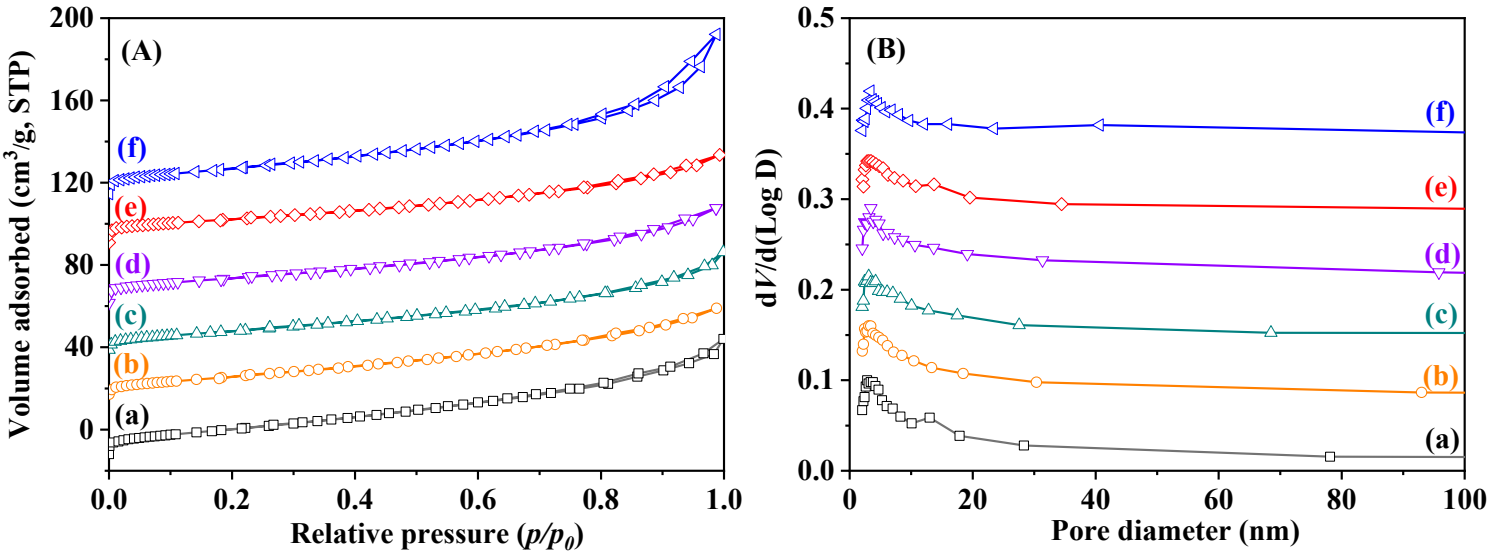



**Figure S2.** (**A**) Nitrogen adsorption–desorption isotherms and (**B**) pore-size distributions of (**a**) $\alpha$-$MnO_2$, (**b**) 0.92Pd/$\alpha$-$MnO_2$, (**c**) 0.91Pt/$\alpha$-$MnO_2$, (**d**) 0.23Pd-0.21Pt/$\alpha$-$MnO_2$, (**e**) 0.47Pd-0.46Pt/$\alpha$-$MnO_2$, and (**f**) 0.93Pd-0.89Pt/$\alpha$-$MnO_2$.

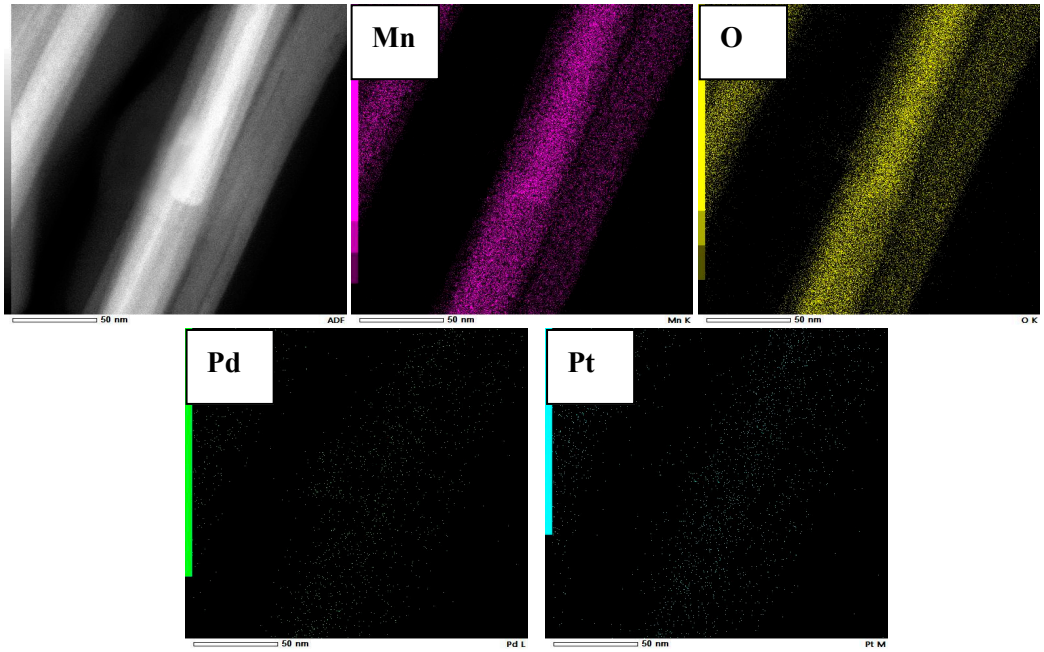



**Figure S3.** HAADF–STEM images and EDS elemental mappings of the 0.47Pd-0.46Pt/$\alpha$-$MnO_2$ sample.

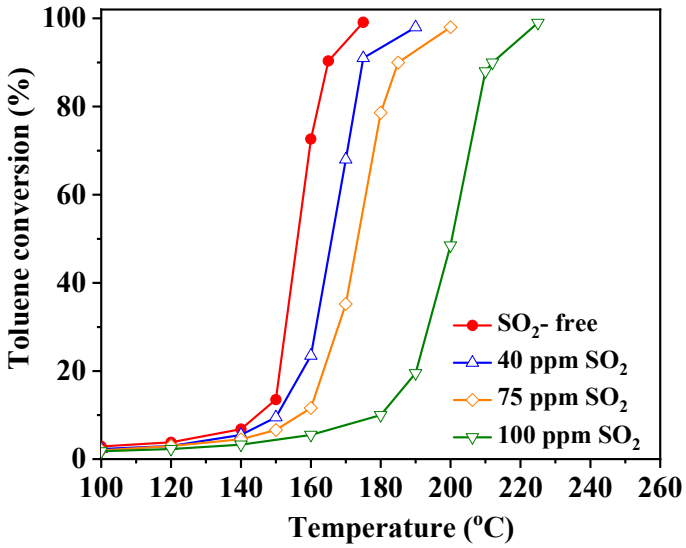



**Figure S4.** Effects of 40, 75 or 100 ppm $SO_2$ on catalytic activity of the 0.47Pd-0.46Pt/$\alpha$-$MnO_2$ sample for toluene oxidation at SV = 60,000 mL/(g h).

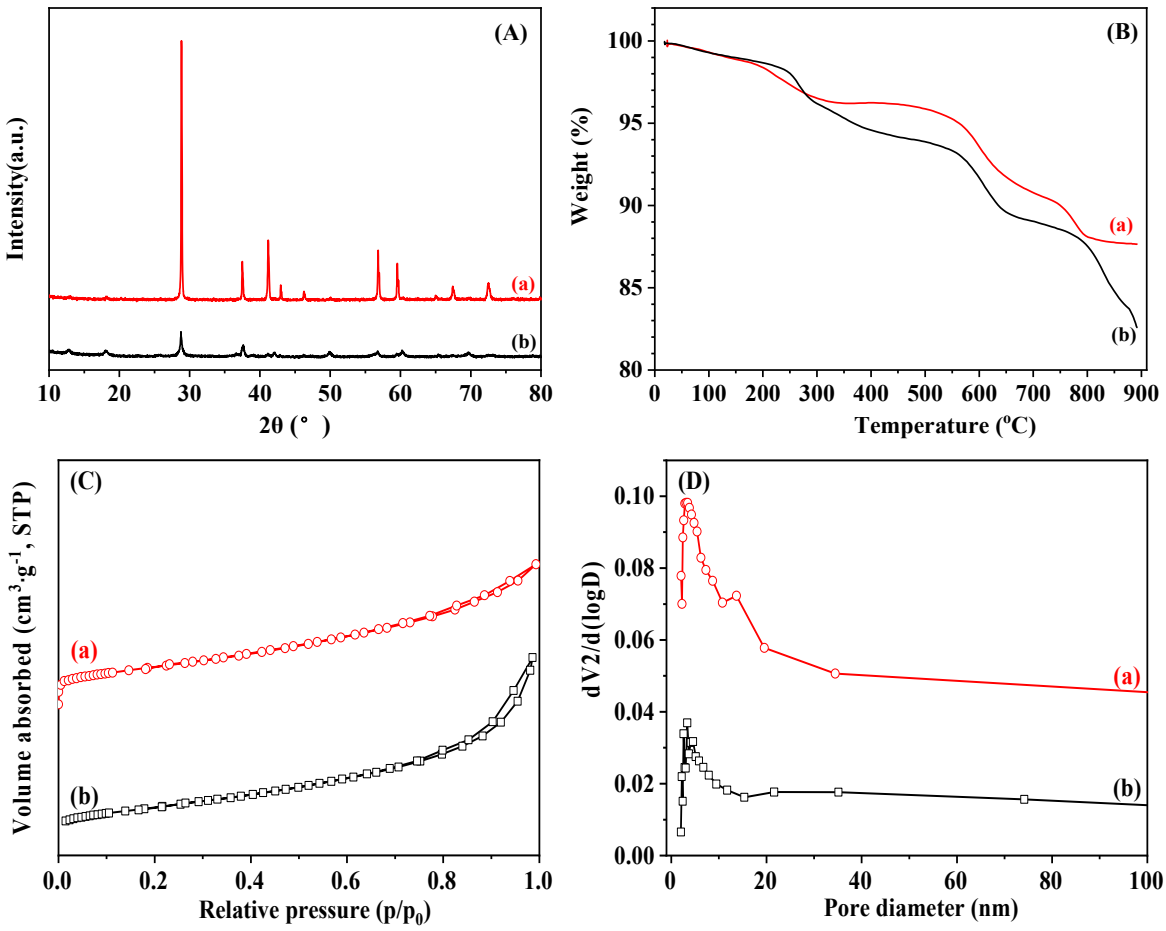



**Figure S5.** (**A**) XRD patterns, (**B**) TG profiles, (**C**) nitrogen adsorption–desorption isotherms, and (**D**) pore-size distributions of the (**a**) fresh 0.47Pd-0.46Pt/$\alpha$-$MnO_2$ sample and (**b**) $SO_2$-treated 0.47Pd-0.46Pt/$\alpha$-$MnO_2$-S sample.

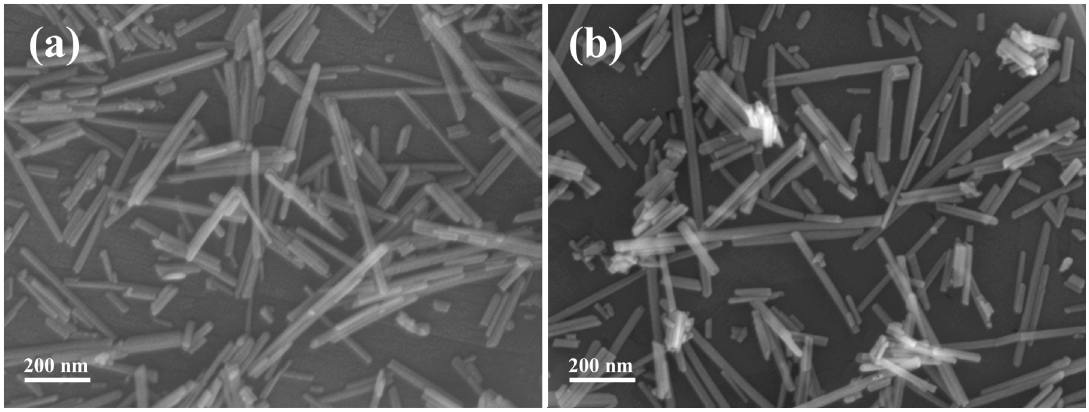



**Figure S6.** SEM images of the (**a**) fresh 0.47Pd-0.46Pt/$\alpha$-$MnO_2$ sample and (**b**) $SO_2$-treated 0.47Pd-0.46Pt/$\alpha$-$MnO_2$-S sample.

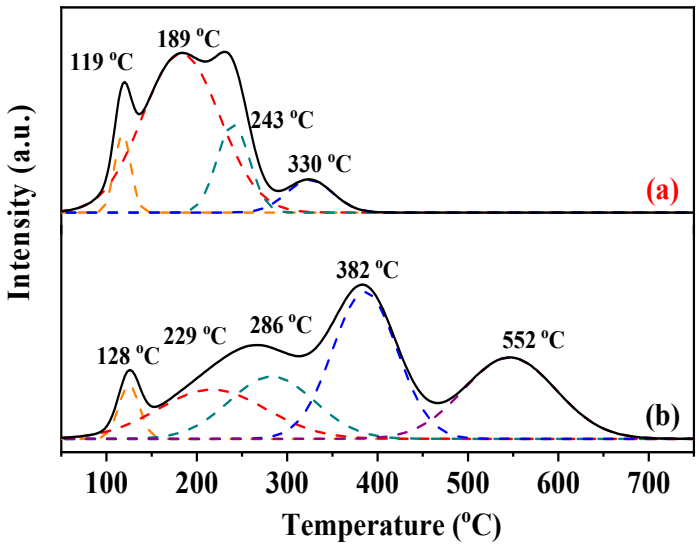



**Figure S7.** $H_2$-TPR profiles of the (**a**) fresh 0.47Pd-0.46Pt/$\alpha$-$MnO_2$ sample and (**b**) $SO_2$-treated 0.47Pd-0.46Pt/$\alpha$-$MnO_2$-S sample.

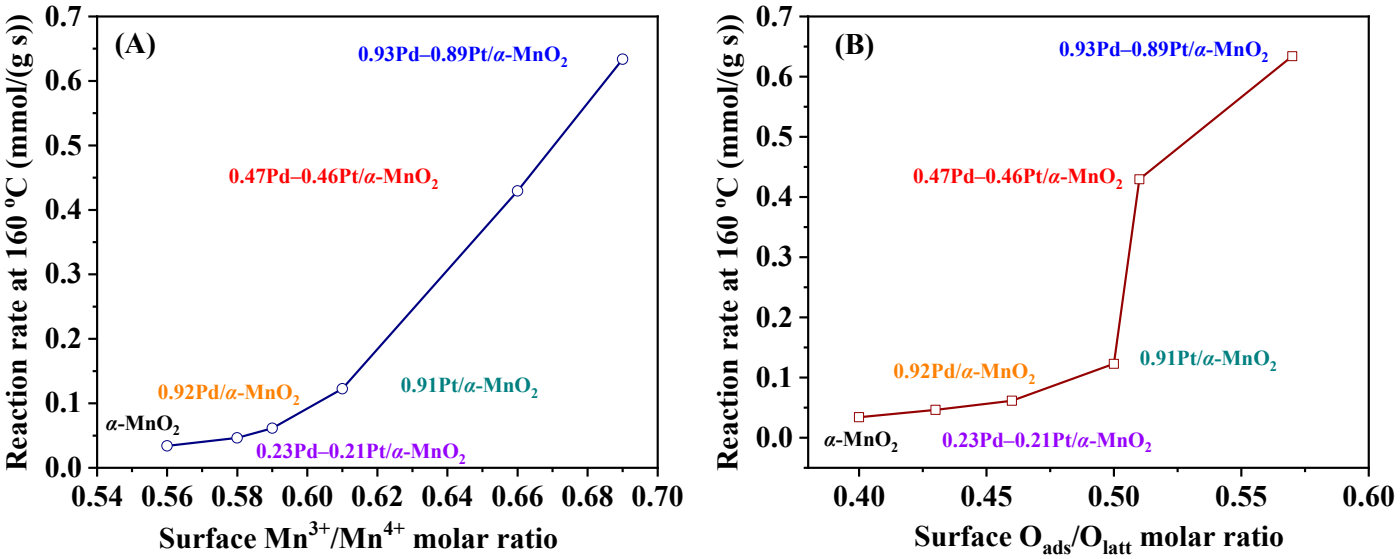



**Figure S8.** Toluene oxidation rate at 160 °C as a function of (**A**) $Mn^{3+}/Mn^{4+}$ or (**B**) $O_{ads}/O_{latt}$ molar ratio of the as-prepared samples.

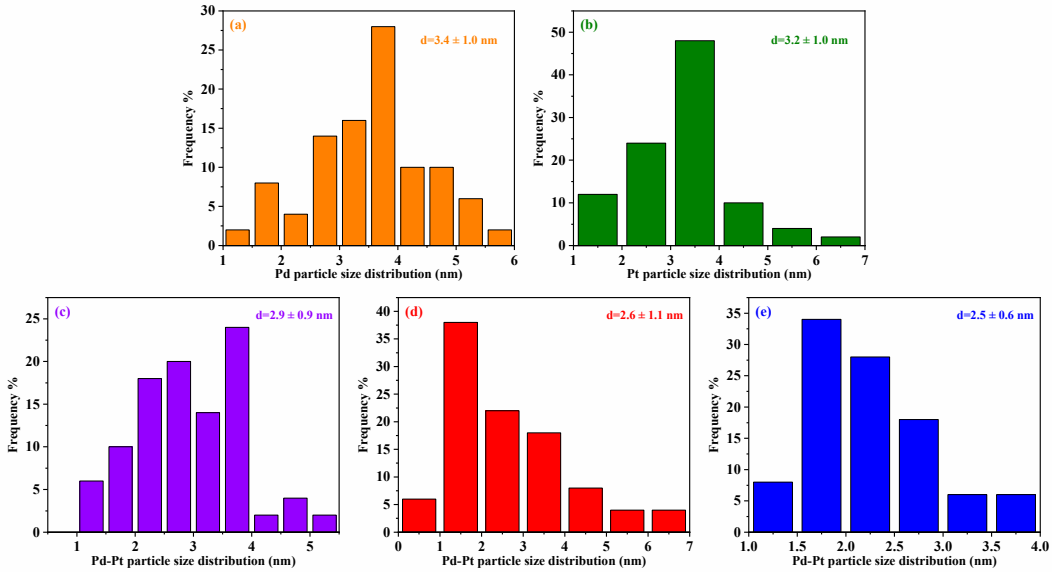



**Figure S9.** Noble particle-size distributions of (**a**) 0.92Pd/$\alpha$-$MnO_2$, (**b**) 0.91Pt/$\alpha$-$MnO_2$, (**c**) 0.23Pd-0.21Pt/$\alpha$-$MnO_2$, (**d**) 0.47Pd-0.46Pt/$\alpha$-$MnO_2$, and (**e**) 0.93Pd-0.89Pt/$\alpha$-$MnO_2$.

**Table S1**. Deconvolution parameters of the Pt 4f XPS spectra of the samples.

| Sample | Binding energy (eV ) | Peak height | FWHM |
|---|---|---|---|
| 0.91Pt/α-$MnO_2$ | 71.3 | 953 | 1.6 |
| | 72.5 | 570 | 1.7 |
| | 74.3 | 1891 | 1.6 |
| | 75.5 | 803 | 1.7 |
| 0.23Pd-0.21Pt/α-$MnO_2$ | 71.3 | 645 | 1.6 |
| | 72.5 | 263 | 1.7 |
| | 74.3 | 676 | 1.6 |
| | 75.5 | 335 | 1.7 |
| 0.47Pd-0.46Pt/α-$MnO_2$ | 71.3 | 433 | 1.6 |
| | 72.5 | 251 | 1.7 |
| | 74.3 | 649 | 1.6 |
| | 75.5 | 279 | 1.7 |
| 0.93Pd-0.89Pt/α-$MnO_2$ | 71.3 | 465 | 1.6 |
| | 72.5 | 254 | 1.7 |
| | 74.3 | 556 | 1.6 |
| | 75.5 | 272 | 1.7 |
| 0.47Pd-0.46Pt/α-$MnO_2$-S | 71.3 | 486 | 1.6 |
| | 72.5 | 195 | 1.7 |
| | 74.3 | 721 | 1.6 |
| | 75.5 | 336 | 1.7 |

**Table S2**. Deconvolution parameters of the Pd 3d XPS spectra of the samples.

| Sample | Binding energy (eV ) | Peak height | FWHM |
|---|---|---|---|
| 0.92Pd/α-$MnO_2$ | 336.5 | 4227 | 1.8 |
| | 337.8 | 2936 | 1.7 |
| | 341.6 | 1409 | 1.8 |
| | 342.6 | 1174 | 1.7 |
| 0.23Pd-0.21Pt/α-$MnO_2$ | 336.5 | 853 | 1.8 |
| | 337.8 | 597 | 1.7 |
| | 341.6 | 470 | 1.8 |
| | 342.6 | 294 | 1.7 |
| 0.47Pd-0.46Pt/α-$MnO_2$ | 336.5 | 950 | 1.8 |
| | 337.8 | 742 | 1.7 |
| | 341.6 | 599 | 1.8 |
| | 342.6 | 436 | 1.7 |
| 0.93Pd-0.89Pt/α-$MnO_2$ | 336.5 | 751 | 1.8 |
| | 337.8 | 602 | 1.7 |
| | 341.6 | 397 | 1.8 |
| | 342.6 | 335 | 1.7 |
| 0.47Pd-0.46Pt/α-$MnO_2$-S | 336.5 | 677 | 1.8 |
| | 337.8 | 558 | 1.7 |
| | 341.6 | 420 | 1.8 |
| | 342.6 | 301 | 1.7 |

**Table S3**. Deconvolution parameters of the Mn 2p XPS spectra of the samples.

| Sample | Binding energy (eV ) | Peak height | FWHM |
|---|---|---|---|
| α-$MnO_2$ | 640.6 | 5936 | 1.7 |
| | 641.9 | 51605 | 1.7 |
| | 643.1 | 87118 | 1.8 |
| 0.92Pd/α-$MnO_2$ | 640.6 | 14492 | 1.7 |
| | 641.9 | 52864 | 1.7 |
| | 643.1 | 84406 | 1.8 |
| 0.91Pt/α-$MnO_2$ | 640.6 | 16837 | 1.7 |
| | 641.9 | 45348 | 1.7 |
| | 643.1 | 70518 | 1.8 |
| 0.23Pd-0.21Pt/α-$MnO_2$ | 640.6 | 14279 | 1.7 |
| | 641.9 | 55824 | 1.7 |
| | 643.1 | 90610 | 1.8 |
| 0.47Pd-0.46Pt/α-$MnO_2$ | 640.6 | 19551 | 1.7 |
| | 641.9 | 59367 | 1.7 |
| | 643.1 | 84722 | 1.8 |
| 0.93Pd-0.89Pt/α-$MnO_2$ | 640.6 | 16731 | 1.7 |
| | 641.9 | 55261 | 1.7 |
| | 643.1 | 75990 | 1.8 |
| 0.47Pd-0.46Pt/α-$MnO_2$-S | 640.6 | 16627 | 1.7 |
| | 641.9 | 47006 | 1.7 |
| | 643.1 | 75724 | 1.8 |

**Table S4**. Deconvolution parameters of the O 1s XPS spectra of the samples.

| Sample | Binding energy (eV ) | Peak height | FWHM |
|---|---|---|---|
| α-$MnO_2$ | 529.7 | 110963 | 1.5 |
| | 531.4 | 41560 | 1.6 |
| | 532.7 | 16006 | 1.5 |
| 0.92Pd/α-$MnO_2$ | 529.7 | 90305 | 1.5 |
| | 531.4 | 38481 | 1.6 |
| | 532.7 | 16025 | 1.5 |
| 0.91Pt/α-$MnO_2$ | 529.7 | 81900 | 1.5 |
| | 531.4 | 38377 | 1.6 |
| | 532.7 | 12788 | 1.5 |
| 0.23Pd-0.21Pt/α-$MnO_2$ | 529.7 | 96972 | 1.5 |
| | 531.4 | 38711 | 1.6 |
| | 532.7 | 13524 | 1.5 |
| 0.47Pd-0.46Pt/α-$MnO_2$ | 529.7 | 88837 | 1.5 |
| | 531.4 | 42417 | 1.6 |
| | 532.7 | 12541 | 1.5 |
| 0.93Pd-0.89Pt/α-$MnO_2$ | 529.7 | 84906 | 1.5 |
| | 531.4 | 41190 | 1.6 |
| | 532.7 | 12772 | 1.5 |
| 0.47Pd-0.46Pt/α-$MnO_2$-S | 529.7 | 61843 | 1.5 |
| | 531.4 | 26104 | 1.6 |
| | 532.7 | 9643 | 1.5 |